NANOMATERIALS

3D nanoprinting of semiconductor quantum dots by photoexcitation-induced chemical bonding

Shao-Feng Liu[1]†, Zheng-Wei Hou[2]†, Linhan Lin[1]*, Fu Li[3], Yao Zhao[1], Xiao-Ze Li[1], Hao Zhang[3], Hong-Hua Fang[1], Zhengcao Li[2], Hong-Bo Sun[1,4]*

Three-dimensional (3D) laser nanoprinting allows maskless manufacturing of diverse nanostructures with nanoscale resolution. However, 3D manufacturing of inorganic nanostructures typically requires nanomaterial-polymer composites and is limited by a photopolymerization mechanism, resulting in a reduction of material purity and degradation of intrinsic properties. We developed a polymerization-independent, laser direct writing technique called photoexcitation-induced chemical bonding. Without any additives, the holes excited inside semiconductor quantum dots are transferred to the nanocrystal surface and improve their chemical reactivity, leading to interparticle chemical bonding. As a proof of concept, we printed arbitrary 3D quantum dot architectures at a resolution beyond the diffraction limit. Our strategy will enable the manufacturing of free-form quantum dot optoelectronic devices such as light-emitting devices or photodetectors.
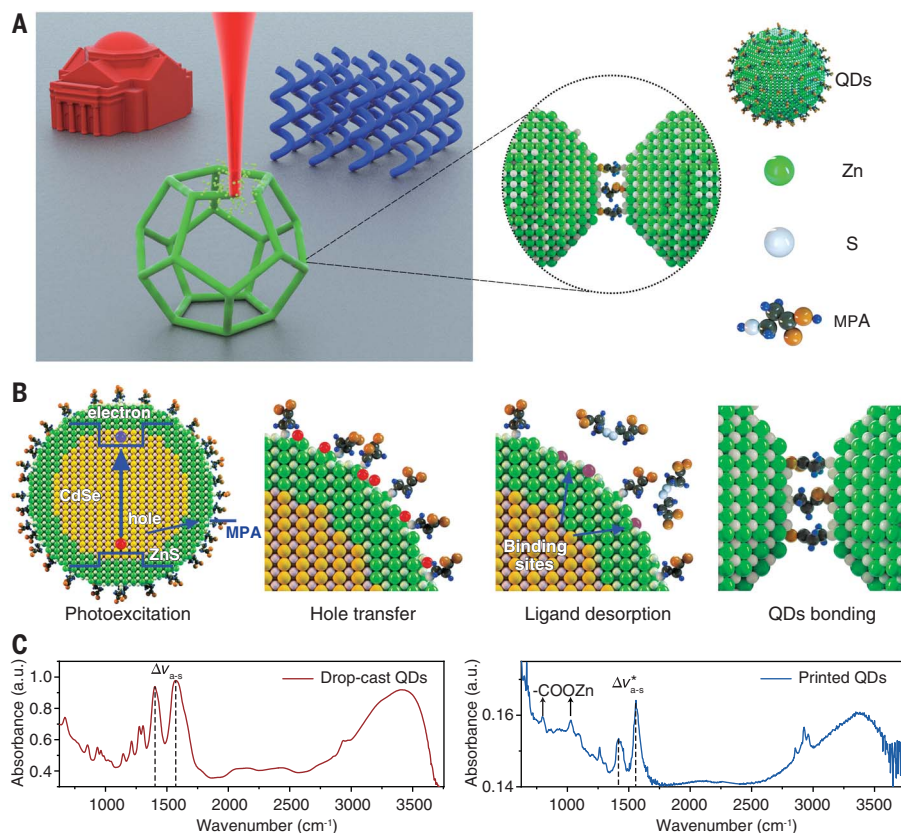
L aser-based nanoprinting features high resolution down to nanometer scale (1–3), but it generally relies on photopolymerization and is limited to photocurable resin. Three-dimensional (3D) manufacturing of functional nanomaterials beyond polymers remains challenging. One strategy is to use a 3D polymer skeleton as a mask for conformal deposition of inorganic materials, producing organic-inorganic nanohybrids (4–6). However, the existence of unwanted polymer skeletons reduces the material's purity and impedes their intrinsic mechanical or physical properties. Although the polymer template can be etched off, only hollow inorganic structures can be obtained. Another strategy is to mix photocurable monomers with inorganic nanomaterials, i.e., photocurable nanocomposites, for direct laser printing (7–9). The cured polymer can be removed by postsintering, but this leads to structural shrinkage and defect generation (10–12).

The key to resolving these problems is to develop a printing mechanism beyond photopolymerization. Talapin et al. designed photoactive ligands that decompose under light irradiation for direct optical lithography (13). However, this method requires the sophisticated design of surface ligands that are selective to specific nanocrystals. In the present work, taking semiconductor quantum dots (QDs) as an example, we propose a strategy that

uses electron-hole pairs generated by photoexcitation to modify the surface chemistry of QDs to induce interparticle chemical bonding, which we call photoexcitation-induced chemical bonding (PEB). Figure 1A illustrates the design concept. Semiconductor QDs were used because they are able to generate electron-hole

pairs under excitation. Such high-energy carriers, once captured or trapped, can modify the local electronic states and tune the chemical reactivity for interparticle bonding.

To demonstrate this concept, we chose water-phase colloidal CdSe/ZnS core/shell QDs capped with 3-mercaptopropionic acid (MPA) as an example (figs. S1 to S3). The MPA molecules are connected to the ZnS shell through Zn–S bonds, with the carboxyl groups exposed to environmental water. Under laser excitation, the excitons generated inside the CdSe core have three decay channels: radiative recombination, nonradiative recombination, and electron-hole pair dissociation to form separated electrons and holes (14), the latter of which plays a substantial role in PEB. Because the highest occupied molecular orbital (HOMO) of MPA molecules is located above the valence band maximum (VBM) of CdSe (Fig. 1B), the generated holes will tunnel through the outer potential barrier and transfer to the nanocrystal surface (see supplementary text S1 for a detailed analysis) (15–17). A thin shell thickness and a small energy difference of core/shell valence bands are preferred to increase the tunneling probability. Specially, the thiol groups on the nanocrystal surface

[1]State Key Laboratory of Precision Measurement Technology and Instruments, Department of Precision Instrument, Tsinghua University, Haidian, Beijing 100084, China. [2]Key Laboratory of Advanced Materials (MOE), School of Materials Science and Engineering, Tsinghua University, Haidian, Beijing 100084, China. [3]Department of Chemistry, Tsinghua University, Haidian, Beijing 100084, China. [4]State Key Laboratory of Integrated Optoelectronics, College of Electronic Science and Engineering, Jilin University, Changchun 130012, China.
*Corresponding author. Email: linlh2019@mail.tsinghua.edu.cn (L.L.); hbsun@tsinghua.edu.cn (H.-B.S.)
†These authors contributed equally to this work.

Fig. 1. Working principle of PEB. (**A**) Schematic illustration showing 3D nanoprinting of MPA-capped CdSe/ZnS QDs using PEB. (**B**) Schematic illustration showing the underlying mechanism of PEB. (**C**) FTIR spectra of the drop-cast QDs and printed structure.

strongly influence the electron and hole wavefunctions and affect the charge-transfer process (18). The surface MPA ligands capture the holes, desorb from the surface, and form dissolved disulfides in the solution (16, 19):

$$2Zn - S - R + 2h^+ \rightarrow RSSR + 2Zn^+$$

$$(R = CH_2-CH_2-COO^-) \quad (1)$$
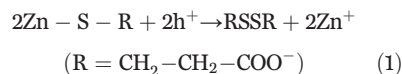
where Zn^+ refers to the zinc atoms on the nanocrystal surface after ligand desorption. Such exposed zinc atoms are active bonding sites that are connected to the COO^- group from the nearby QDs for interparticle bonding. In addition to the CdSe/ZnS core/shell QDs, this concept can be extended to other semiconductor nanomaterials such as MPA-capped CdSe and CdS QDs (fig. S4) because the VBM of these QDs is below the HOMO of MPA. By contrast, it cannot work for MPA-capped InP/ZnS QDs because the VBM of InP is higher than the HOMO of MPA (fig. S5 and table S1). PEB is also applicable to metallic nanoparticles once the generated hot carriers have sufficiently high energy to transfer to the nanocrystal surface and drive ligand desorption (see fig. S6 for the printing of MPA-capped silver nanoparticles).

To understand the PEB process, we conducted Fourier transform infrared (FTIR) spectroscopy on both drop-cast QDs and printed species (Fig. 1C). The peaks between 1300 and 1600 cm^{-1} correspond to the symmetric and asymmetric stretching modes of deprotonated carboxylate COO^- groups in MPA ligands (20). Although these peaks are observable in both samples, the frequency separations ($\Delta\nu_{a-s}$) between the symmetric and asymmetric stretching modes decrease from 170.5 cm^{-1} (drop-cast QDs) to 140.6 cm^{-1} (printed QDs), revealing that COO^- groups are bounded to the nanoparticle surface through bidentate bridging (21). Moreover, two new peaks appear at ~800 and 1030 cm^{-1} in the printed sample, corresponding to the weak vibrations of Zn–O bond and stretching vibrations of C–O groups in zinc acetate, respectively, which further confirm the formation of COO-Zn bonds (22, 23). The FTIR results also exclude the possibility of ligand cross-linking or decomposition (see supplementary text S2). Beyond MPA ligands, PEB can also be applied to QDs capped with other surface ligands composed of thiol, such as cysteamine (fig. S7) and glutathione, if their HOMOs are located above the valance band of QDs. However, the applicability on ligands composed of non-thiol head groups is still unclear.

To further verify the underlying mechanism, we conducted a series of control experiments. Taking a 532-nm continuous-wave laser for excitation, the red QDs are excited and printed, whereas no printing occurs for blue QDs. By comparison, we selected a 780-nm

femtosecond laser for two-photon excitation and observed that all the blue, green, and red QDs got printed. Moreover, we ruled out the contribution of optical force (movie S1, fig. S8, and supplementary text S3) and photothermal effect (figs. S9 and S10 and supplementary text S4) in initiating the printing process.

PEB is a substrate-independent technique, and we can create suspended QD assembly in the solution, indicating potential 3D nanoprinting capability. As a proof of concept, we sealed the QD dispersions in a homemade chamber ~50 μm in thickness with a cleaned sapphire substrate on the top. By steering the femtosecond laser spot location, we demonstrate the printing of QDs into various nanopillar patterns. As shown in Fig. 2A, we printed hundreds of nanopillars into the Chinese characters of "Tsinghua University," which exhibit uniform height and fluorescence intensity distribution (fig. S11). The fluorescence intensity of each pixel can be adjusted by controlling the pixel diameter or height (fig. S12). Specifically, the height adjustment allows tuning the fluorescence intensity without variation of printing resolution. As a demonstration, we also printed horse patterns with thousands of nanopixels of different heights (Fig. 2B and fig. S13B). The gap between adjacent nanopillars can be flexibly adjusted to control the integration density (fig. S14). Figure 2C shows the superresolution fluorescence image of the nanopixeled horse pattern with a pixel spacing of ~1000 nm and a pixel size of ~565 nm [>2 × 10^4 dots per inch; also see the scanning electron microscopy (SEM) images in fig. S15]. From the high-magnitude SEM and transmission electron
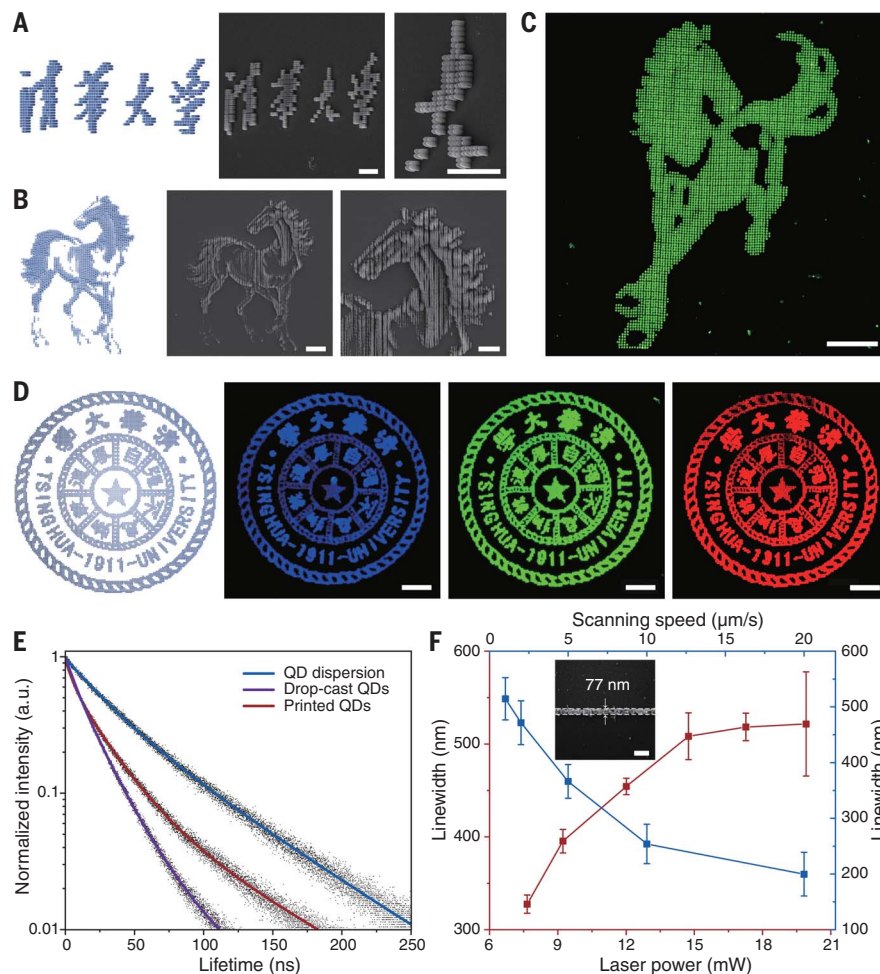
Fig. 2. Nano-pixel printing and QD characterization. (**A**) Model and tilt-view SEM images of the Chinese characters of "Tsinghua University." (**B**) Model and tilt-view SEM images of a horse printed with nanopixels of different heights. (**C**) Superresolution PL image of the nanopixeled horse. (**D**) Model and PL images of the badge of Tsinghua University consisted of QDs emitting blue, green, and red light, respectively. (**E**) PL lifetimes of QD dispersion, drop-cast QDs, and printed QDs. (**F**) Printing linewidths as functions of laser power and scanning speed. Error bars indicate means ± SEM. Scale bars: (A) and (B), right panel, 5 μm; (B), middle panel, 10 μm; (C) and (D), 20 μm; and (F), 200 nm.

microscopy images (figs. S16 to S18), the printed nanocrystals experience a relatively dense distribution. At a low dose, the QDs are bridged with surface ligands and no aggregation is observed. However, at a high dose (e.g., ≥49.1 mJ μm^{-1}), aggregation of QDs is observed because of the large number of desorbed ligands and the induced dispersion instability (see the supplementary text S5 and figs. S19 and S20). The fluorescence lifetime also scales down with the printing dose because of the increased density or formation of large aggregation (fig. S21). Moreover, we measured the photocurrent of the printed materials and obtained a value of ~0.5 nA at an applied voltage of 10 V under illumination of the 385-nm light (optical power density: 18 W/m^2; see supplementary text S6 and fig. S22). The PEB technique paves the way for the fabrication of highly integrated optoelectronic devices such as photodetectors and QD light-emitting diodes.

We further demonstrated the printing of blue, green, and red QDs to represent three primary colors using the badge of Tsinghua University as a model (Fig. 2D and fig. S23). We also compared the photoluminescence (PL) spectra and radiative recombination lifetimes of QD dispersion, drop-cast QDs, and printed QDs. According to the normalized PL spectra, the emission wavelengths between drop-cast and printed QDs are almost the same, whereas both exhibit a slight redshift in comparison with the QD solution (fig. S24). This redshift may arise from the Förster resonant energy transfer between neighboring QDs (24). From the PL lifetimes, we find that the excitons in printed structure first experience a rapid decay caused by ligand-binding–induced trap states and then decay slowly, similar to dispersed QDs in solution (Fig. 2E). The longer lifetime observed in the printed samples indicate that they have a lower density than the drop-cast ones.

As a nanoprinting approach, one of the key parameters is the printing resolution. We investigated the printing linewidths as functions of laser power and scanning speed (Fig. 2F). The linewidth increases rapidly, whereas it levels off above a power threshold of ~15 mW. This can be explained by power-dependent two-photon absorption as the effective absorption area on the focus plane grows rapidly with the laser power and then slows down. By contrast, the printing linewidth scales down with scanning speed because of the reduction of absorbed power. With parameter optimization, the minimum printing linewidth obtained in our experiments is 81 ± 4 nm, with a line edge roughness of 12 ± 2 nm (see the inset of Fig. 2F and fig. S25), which is far beyond the optical diffraction limit. The line edge roughness scales down with the increasing height because more QDs are printed and the irregularity at the edge is smoothed out (fig. S26).

To demonstrate the 3D nanoprinting capability, we programmed the laser beam to scan in 3D space and built a wide range of complex structures across from linear and curved
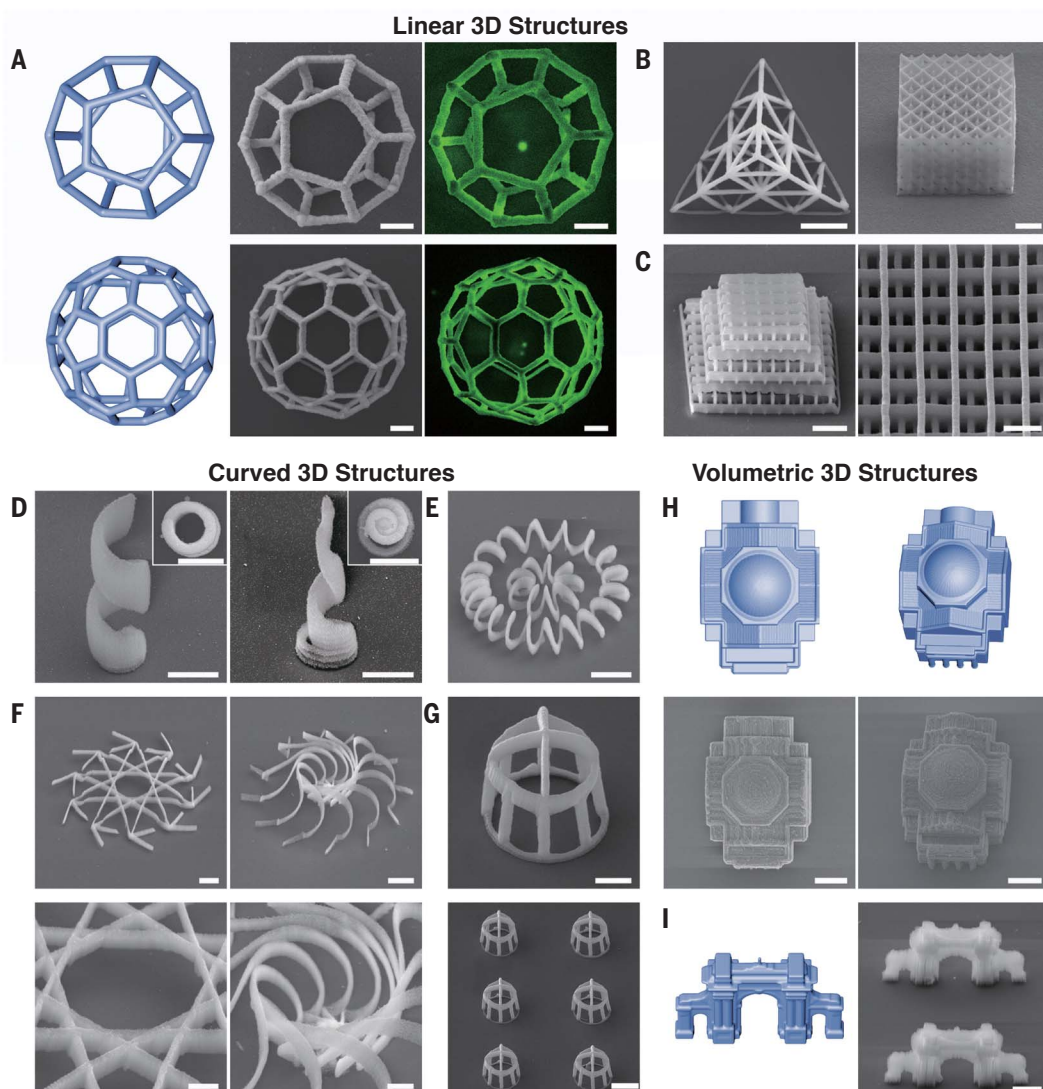
Fig. 3. Linear, curved, and volumetric 3D nanostructures.
(**A**) Models, SEM, and cathodoluminescence images of dodecahedron and C60 lattice, respectively.
(**B**) SEM images of triangular lattice and cubic lattice structures.
(**C**) SEM images of woodpile structures. (**D**) Tilt-view SEM images of upright helices (the inset SEM images show the top view). (**E**) SEM image of a lay-flat helical structure. (**F**) SEM images of nest-like structures with multiple curved lines. (**G**) SEM images of dome structures. (**H**) Models and SEM images of the auditorium at both top view and tilt view. (**I**) Model and tilt-view SEM image of the old gate. Scale bars: (A) and (C), right panel, (D) and (F), bottom panels, (G), top panel, 2 μm; (B) and (C), left panel, (E) and (F), top panels, (G), bottom panel, and (I), 5 μm; and (H), 10 μm.
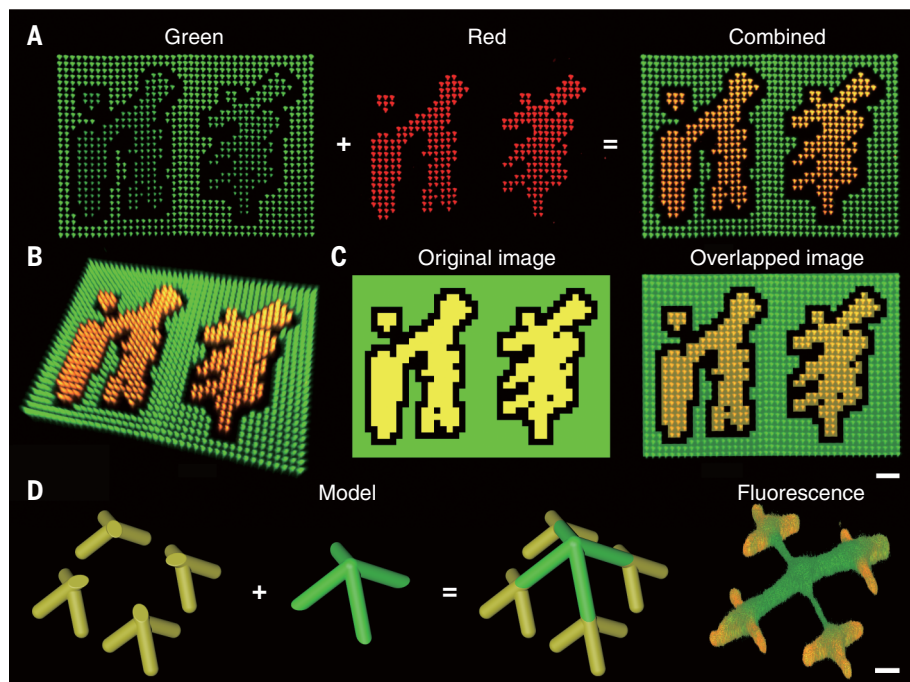
Fig. 4. Multicolor display and heterogeneous printing. (**A**) Fluorescence images of the printed Chinese characters of "Tsinghua University." (**B**) Tilt view of the 3D reconstructed fluorescence image. (**C**) Designed image and its overlap with printed structure. (**D**) Heterogeneous printing of a single 3D structure as illustrated by the model and its reconstructed 3D fluorescence image. Scale bars: (A) to (C), 10 μm; (D), 2 μm.

to volumetric 3D structures. Figure 3A shows the schematics, SEM images, and cathodoluminescence images of a dodecahedron lattice and a C60 lattice. The identical cathodoluminescence intensity from the 3D structures reveals the structural uniformity. We also built a triangular lattice and a cubic lattice, which are mainly composed of slope line components (Fig. 3B). As shown in Fig. 3C, we built 3D woodpile structures with the length of the bottom straight lines at 20 μm and the length-to-width ratio >40. This provides the possibility of fabricating 3D active photonic crystal devices without postprocessing treatment such as pyrolysis or calcination (also see fig. S27).

In addition to the linear 3D structures, we also fabricated various curved 3D structures in freeform. As shown in Fig. 3D, we built helical structures with both equal and ever-changing diameters in each circle. The structures are vertically elongated because of laser intensity distribution above and below the focus plane. Such elongation can be reduced by optimizing the incident light field. We also fabricated a lay-flat helical structure by two single, continuous laser scans (Fig. 3E) and more sophisticated cured 3D nanostructures such as nest-like structures and dome structures (Fig. 3, F and G). The PEB approach also exhibits excellent reproducibility. As shown in Fig. 3G and fig. S28, all of the architectures in the nanoarrays show excellent consistency with

each other (also see movie S2). Moreover, we demonstrated the fabrication of volumetric 3D structures, including the auditorium and the old gate of Tsinghua University, using layer-by-layer scanning (Fig. 3, H and I).

Finally, we demonstrated the heterogeneous printing of different QDs into 3D nanostructures. Specifically, the mixing of QDs allows the tuning of emission color. For instance, we mixed the green and red QDs as feedstock and printed the Chinese characters of Tsinghua University with yellow light emitting. For comparison, we printed green QDs around the yellow characters as the background. Each pixel in the fluorescence images contains three sloped nanopillars with a height of 1 μm. Figure 4A shows the fluorescence images of different parts to depict the printing process, and Fig. 4B shows the 3D reconstructed fluorescence image. The excellent overlap between design and fluorescence image further reveals the high printing accuracy (Fig. 4C). Finally, we demonstrated the printing of a 3D heterogeneous structure composed of four yellow "feet" and a green linker, with the intersection at the top (Fig. 4D). Heterogeneous 3D nanoprinting is very important in the fabrication of multifunctional optoelectronic devices such as full-color 3D nanodisplays in free space.

In summary, taking advantage of the photoexcitation-induced surface chemistry modification and the formation of chemical

bonds, we developed a laser nanoprinting technique to directly assemble dispersed QDs into 3D architectures at high accuracy and high resolution. Without any additives or postprocessing treatment, the PEB technique allows us to maintain the photonic and optoelectronic properties of the QDs during the printing process. Although this concept is demonstrated in semiconductor QDs, it can be potentially extended to non-semiconductor nanomaterials once high-energy carriers can be generated to modify the surface chemistry of the nanoparticles.

REFERENCES AND NOTES

1. S. Kawata, H.-B. Sun, T. Tanaka, K. Takada, *Nature* **412**, 697–698 (2001).
2. V. Hahn et al., *Nat. Photonics* **15**, 932–938 (2021).
3. L. Li, R. R. Gattass, E. Gershgoren, H. Hwang, J. T. Fourkas, *Science* **324**, 910–913 (2009).
4. L. R. Meza, S. Das, J. R. Greer, *Science* **345**, 1322–1326 (2014).
5. A. Issa et al., *ACS Appl. Mater. Interfaces* **13**, 41846–41856 (2021).
6. T. A. Schaedler et al., *Science* **334**, 962–965 (2011).
7. X. Wen et al., *Nat. Mater.* **20**, 1506–1511 (2021).
8. Y. Peng et al., *Adv. Mater. Technol.* **4**, 1800522 (2019).
9. F. Kotz et al., *Adv. Mater.* **33**, e2006341 (2021).
10. A. Desponds et al., *Small* **17**, e2102486 (2021).
11. A. Vyatskikh, R. C. Ng, B. Edwards, R. M. Briggs, J. R. Greer, *Nano Lett.* **20**, 3513–3520 (2020).
12. D. W. Yee, M. L. Lifson, B. W. Edwards, J. R. Greer, *Adv. Mater.* **31**, e1901345 (2019).
13. Y. Wang, I. Fedin, H. Zhang, D. V. Talapin, *Science* **357**, 385–388 (2017).
14. J. Gao, J. Zhang, J. van de Lagemaat, J. C. Johnson, M. C. Beard, *ACS Nano* **8**, 12814–12825 (2014).
15. P. Singhal et al., *Nanoscale* **8**, 1823–1833 (2016).
16. J. Aldana, Y. A. Wang, X. Peng, *J. Am. Chem. Soc.* **123**, 8844–8850 (2001).
17. S. F. Wuister, C. de Mello Donegá, A. Meijerink, *J. Phys. Chem. B* **108**, 17393–17397 (2004).
18. D. A. Hines, P. V. Kamat, *J. Phys. Chem. C* **117**, 14418–14426 (2013).
19. M. J. Natan, J. W. Thackeray, M. S. Wrighton, *J. Phys. Chem.* **90**, 4089–4098 (1986).
20. C. D. Dieleman et al., *Nanoscale* **12**, 11306–11316 (2020).
21. E. R. Kennehan et al., *J. Am. Chem. Soc.* **143**, 13824–13834 (2021).
22. G. Hitkari, S. Singh, G. Pandey, *Nano-Structures & Nano-Objects* **12**, 1–9 (2017).
23. M. Gaidi et al., *J. Solid State Electrochem.* **22**, 3631–3637 (2018).
24. L. Wang et al., *ACS Appl. Mater. Interfaces* **13**, 17861–17868 (2021).

SUPPLEMENTARY MATERIALS

science.org/doi/10.1126/science.abo5345

Science

3D nanoprinting of semiconductor quantum dots by photoexcitation-induced chemical bonding

Shao-Feng LiuZheng-Wei HouLinhan LinFu LiYao ZhaoXiao-Ze LiHao ZhangHong-Hua FangZhengcao LiHong-Bo Sun

Photoprinting nanoparticles

Nanoparticle assembly often requires tailored selection of the ligands so that they can selectively bond, as with complementary DNA strands. Alternately, they can be linked together at specified locations using photopolymerization to connect ligands at desired places. However, this process adds to the complexity of making the nanoparticles and is limited by the fidelity of the ligand attachment. Liu *et al.* show that light can be used to desorb surface thiolate ligands from cadmium selenide/zinc sulfide core shell quantum dots (see the Perspective by Pan and Talapin). The resulting trapped holes drive bonding between the particles through the remaining surface ligands. The authors reveal photoprinting of arbitrary three-dimensional architectures at a resolution beyond the diffraction limit and for a range of nanocrystals. Printing can be optically selected based on the size and/or bandgap of the quantum dots. —MSL

View the article online
https://www.science.org/doi/10.1126/science.abo5345
Permissions
https://www.science.org/help/reprints-and-permissions

Use of this article is subject to the Terms of service